# Discussion of: Design for Local Member Shear at Brace and Diagonal-Member Connections: Full-Height and Chevron Gusset

Original Paper by Rafael Sabelli and Brandt Saxey

Discussion by Paul W. Richards


## ABSTRACT

The paper "Design for Local Member Shear at Brace and Diagonal-Member Connections: Full-Height and Chevron Gusset" (Sabelli and Saxey, 2021) develops equations for checking local member shear demands using a Concentrated Stress Method (CSM) and presents a design example. This discussion presents results from a finite element (FE) model, based on the design example in the paper, to quantify the accuracy of the proposed design equations in predicting beam yielding. The FE model confirmed that the beam yielding state would not have occurred for the example frame under the design forces but would have occurred for forces about 4% higher. The stress and strain distributions observed in the FE model were consistent with those assumed in the CSM, although two points for potential refinement were noted. If beam yielding in a concentrically braced frame is forced, through oversized braces, the plastic mechanism would be like an eccentrically braced frame (EBF) but with higher yield force and higher beam inelastic rotations and strains for the same inelastic story drift.


## INTRODUCTION

The paper being discussed is one of several articles that have appeared in the AISC *Engineering Journal* addressing local member shear demands in braced frames (Fortney and Thornton, 2015, 2017; Fortney, 2020; Hadad and Thornton, 2022; Roeder et al., 2021; Sabelli and Bolin, 2022; Sabelli and Saxey, 2021; Sabelli et al., 2021). In the paper, the authors develop equations for checking local member shear demands in braced frames using a Concentrated Stress Method (CSM) and present a design example.

Figure 1 shows braced frames with different governing limit states. For seismic design, it is the intent of the *Seismic Provisions for Structural Steel Buildings* (AISC, 2016) that a brace yielding limit state govern [Figure 1(a)]. For nonseismic design, it could be fine for a beam shear yielding limit state to govern [Figure 1(b)], but the limit state needs to be checked explicitly to ensure that it is not reached under the design loads. Sabelli and Saxey (2021) outline the procedure for checking this beam shear yielding limit state [Figure 1(b)]. In their design example of a seismic frame, they use CSM to check beam yielding [Figure 1(b)] in order to ensure that brace yielding actually governs [Figure 1(a)].


Paul Richards, Vice President of Research and Development, DuraFuse Frames, West Jordan, Utah. Email: paul.richards@durafuseframes.com



Paper No. 2021-01D


In the paper, the authors cite previous work where finite element models were used to investigate beam shear demands in chevron frames (Richards et al., 2018). While results from those finite element (FE) models were consistent with the CSM design method, those FE models were somewhat limited in their ability to predict post-yield behavior.

The publication of Sabelli and Saxey (2021), including their thorough design example (CSM example), provided an opportunity for more robust FE validation. To determine the accuracy of their equations for checking beam shear yielding, FE analysis was performed on a model based on their design example. In the CSM example, the beam was capacity-designed based on the maximum forces that could be delivered by the braces [Figure 1(a)], but in the FE model, the braces were given unlimited strength to force the beam shear yielding mechanism [Figure 1(b)] to develop. The FE model answered three questions:

- Was the CSM used by Sabelli and Saxey (2021) accurate?
- What load would have caused shear yielding in the beam?
- What would have happened if a beam shear mechanism developed?

The answers to the first two questions are pertinent for new design. The answer to the last may be pertinent for some existing braced-frames where beam local shear yielding was not checked during design.

This discussion will describe the FE model and discuss the CSM example in the context of the FE model results.

## FINITE ELEMENT MODEL

The geometry of the FE model matched that of the CSM example [Figure 2(a)]. The example frame connection had a W24×94 beam with gussets that had a 0.75 in. thickness and a 56 in. effective length (the gusset was 58 in. long, but the weld was held back 1 in. from each end). The four braces framing into the beam had an angle of 50.2° off horizontal. Figure 1(b) shows the maximum expected brace forces. The horizontal components in the lower story sum to 782 kips. The gusset was proportioned to be just long enough to preclude beam shear yielding under these forces (based on the CSM). The gusset-to-beam welds were ½ in. for the end segments (14 in. each end) and 5⁄16 in. for the 28 in. in the middle.

The FE model was developed and analyzed with ANSYS (2022). Three types of elements were used in the model to represent various components efficiently. The gusset plates, brace ends, welds, and beam (in the connection region) were

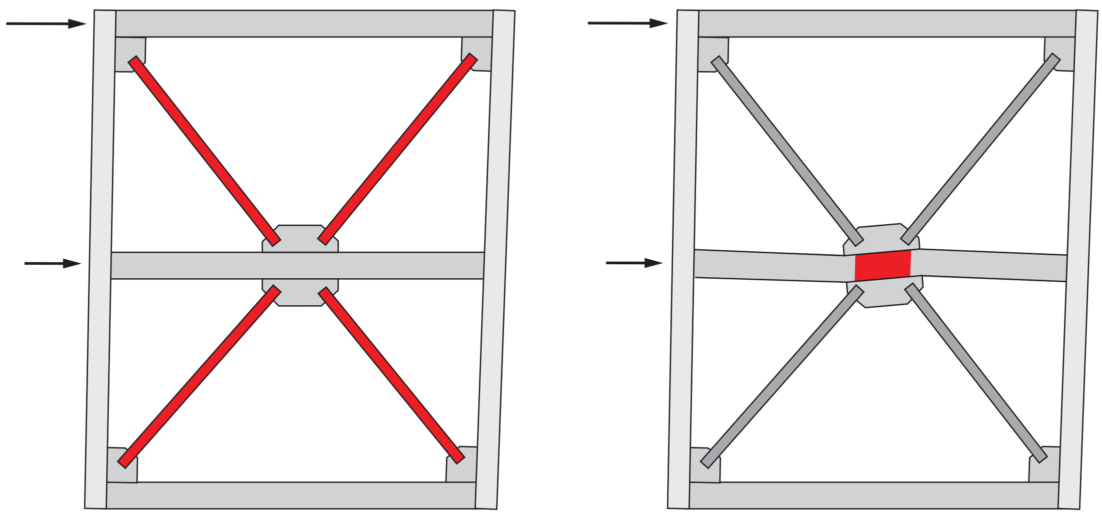

*(a) Brace tension/compression yielding* *(b) Beam shear yielding*

*Fig. 1. Braced frames with different governing limit states.*

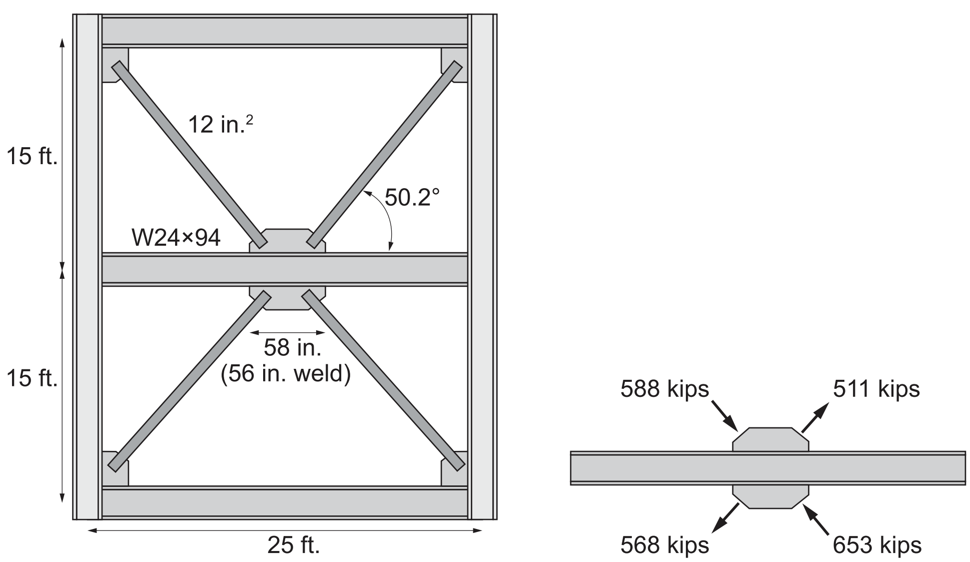


*(a) Geometry* *(b) Design loads*

*Fig. 2. Frame from the CSM example.*

modeled with solid elements (SOLID186) [Figure 3(a)-(c)]. The beam mesh in the connection region had an element dimension of 1 in. [Figure 3(b)]. The gusset-to-beam welds were modeled explicitly [Figure 3(c)]. Outside the gusset region, the beam was represented with elastic beam elements (BEAM188) [Figure 3(a)] with the cross-sectional properties of a W24×94. The braces were represented with elastic truss elements (LINK180) to force the beam shear yielding mechanism to form. Effective areas were used for the brace elements so that the magnitudes of the brace forces (relative to each other) would match the relative magnitudes of the forces in the design example [Figure 2(b)].

The boundary conditions and loading in the model were for a pushover-type analysis [Figure 3(a)]. The bottom nodes of the bottom braces were pinned in space. The beam ends and top brace nodes were on rollers that prevented movement in the *y*-direction and had displacements imposed in the *x*-direction. The relative magnitudes of the top and bottom applied displacements [0.526*x* in Figure 3(a)] were calibrated so that the magnitudes of the brace forces in the two stories would match the relative magnitudes of the forces in the design example [Figure 2(b)]. Out-of-plane restraint was applied to all nodes, including the beam web and gusset.

The materials in the FE model simulated nominal steel and weld properties. In the CSM example, the beam and gusset were Grade 50 material. In the FE model, the gusset and beam material had an elastic modulus of 29,000 ksi, a Poisson's ratio of 0.3, a yield stress of 50 ksi, and a post-yield modulus of 290 ksi (1% of elastic). A capping stress of 65 ksi was set, after which the material had negligible further hardening. The weld material in the FE model had an elastic modulus of 29,000 ksi, a yield stress of 70 ksi, and negligible further hardening. These material models, with nominal material strengths, were appropriate for comparison with design procedures that assumed nominal material strength.

The FE model was pushed to a point beyond where the beam shear mechanism was fully developed. Figure 4 shows the pushover curve, where the lateral force is the total applied load on the frame. Figure 4 shows six particular load points, and Table 1 summarizes the significance of each point. Figures 5 through 9 show stress and strain information corresponding to those particular points.

The evolution of the von Mises stress is shown in Figure 5. At a load of 616 kips [Figure 5(a)], there was a region of the beam web at midspan where the von Mises stress exceeded 50 ksi. This region propagated until it reached the extents of the gusset around 815 kips [Figure 5(d)]. At 873 kips [Figure 5(e)], the von Mises stress exceeded 50 ksi for a continuous region of the gusset plate between brace ends. The von Mises plot at 1024 [Figure 5(f)] shows regions with stresses over 55 ksi, reflecting strain hardening.

The evolution of the plastic strains is shown in Figures 6 and 7. At a load of 616 kips [Figure 6(a)], there were no plastic strains greater than 0.002. At 782 kips [Figure 6(c)], localized plastic strains in the beam coalesced to form a full-depth region of the beam web at midspan with plastic strain over 0.002. This plastic region expanded toward the gusset edges. At 873 kips [Figure 6(e)], most of the beam in the gusset region was plastic, as well as a region of the bottom gusset plate between the braces. Figure 7 shows closeup views of the gusset-to-beam weld at the same points. At 1024 kips [Figure 7(f)], the plastic regions of the weld extended 4 in. in from the ends of the weld (beam elements have a 1 in. dimension in the figure), and peak plastic strains exceeded 0.1.

Figure 8 shows the evolution of the shear stresses in the beam and gussets. In the beam, the shear stress exceeded

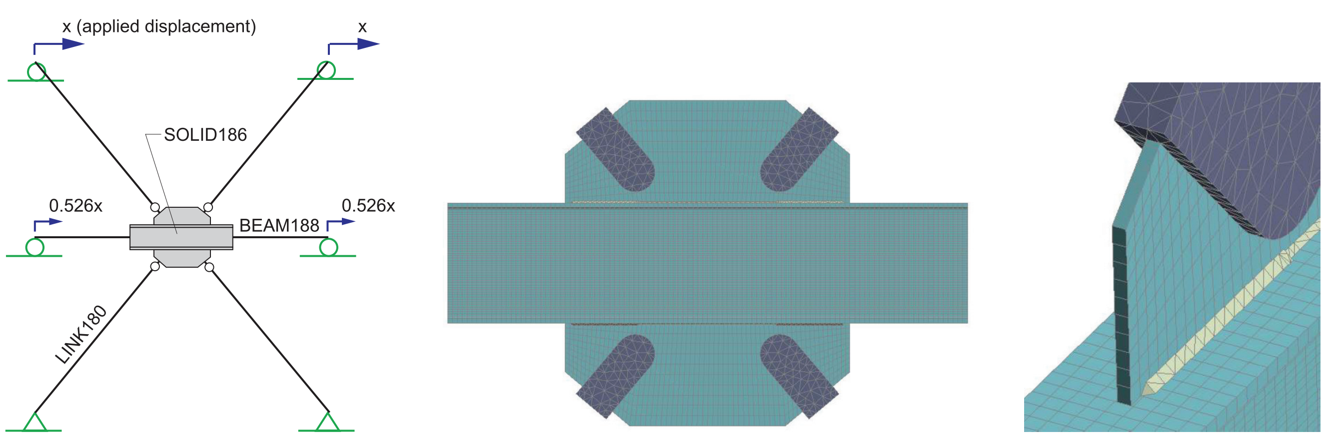


*(a) Element types and boundary conditions*

*(b) Solid element mesh in the connection region*

*(c) Explicit modeling of the welds*

*Fig. 3. Finite element modeling techniques.*

| Table 1. Pushover Points for Discussion | | |
|---|---|---|
| Point | Load (kips) | Significance |
| a | 616 | Von Mises stress exceeded 50 ksi in a localized region of the beam web. |
| b | 744 | Localized plastic strains exceeded 0.002 in the beam web and gusset-to-beam welds. |
| c | 782 | Localized plastic strains in the beam, over 0.002, coalesced to a full-depth region of the beam web. |
| d | 815 | Von Mises stress exceeded 50 ksi for a continuous region between braces in the bottom gusset. Change in tangent stiffness. |
| e | 873 | Shear stresses exceeded 30 ksi ($0.6F_y$) for a full-depth region of the beam web. |
| f | 1024 | Maximum load was applied. |

25 ksi at midspan when the applied lateral load was 616 kips [Figure 8(a)], and the elevated region expanded as the loads increased. However, the shear stress in the beam web did not exceed 30 ksi through an entire section until the load was 873 kips [Figure 8(e)].

At all stages of loading, the shear stresses in the gusset were highest at midspan and decreased near the gusset ends. In fact, the shear stresses changed sign in the regions at the end of the gusset [Figure 8; signs changed at interface of light blue and medium blue], a finding that was documented in Richards et al. (2018). The gusset locations where the shear stress changed sign corresponded with the regions with high normal stress (Figure 9).

Figure 9 shows the evolution of $y$-direction normal stresses in the beam and gussets, which were generally low. For most regions, the normal stresses were between ±20 ksi throughout loading. For loading of 744 kips and above [Figure 9(b)–(f)], regions of concentrated normal stress (above 20 ksi) developed at the ends of the gusset plates. Normal stresses above 50 ksi developed at the highest levels of loading considered.

## DISCUSSION

In the CSM example, the effective gusset length of 56 in. was selected to preclude beam yielding under a lateral force of 782 kips (the maximum force that could be delivered by the braces). If the CSM were accurate, the beam shear yielding limit state would be observed in the FE model at a load slightly greater than 782 kips.

The results in Figure 4 through 10 indicate that the beam shear yielding limit state was reached at a load a little greater than 782 kips. The pushover plot (Figure 4) shows softening around 782 kips that continued to develop

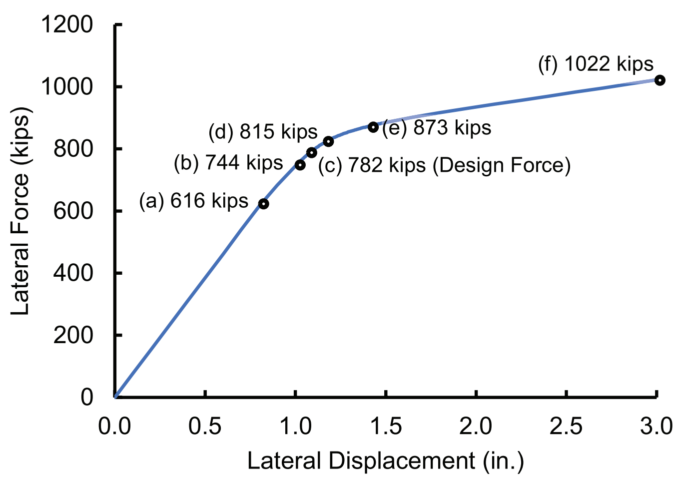


*Fig. 4. Pushover curve for the finite element model.*

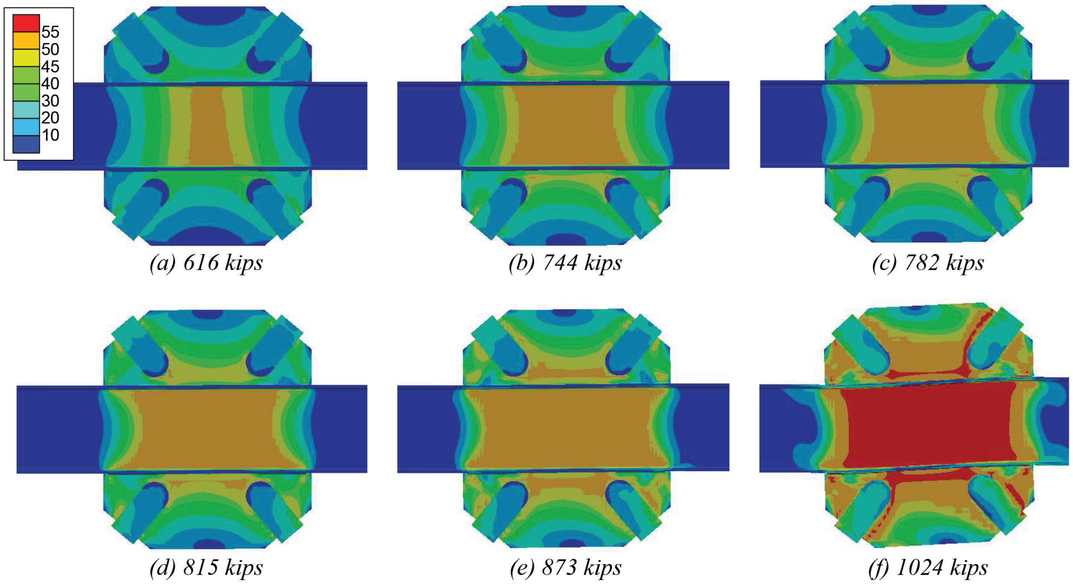


*Fig. 5. Equivalent (von Mises) stress (ksi) contours in the beam and gussets.*

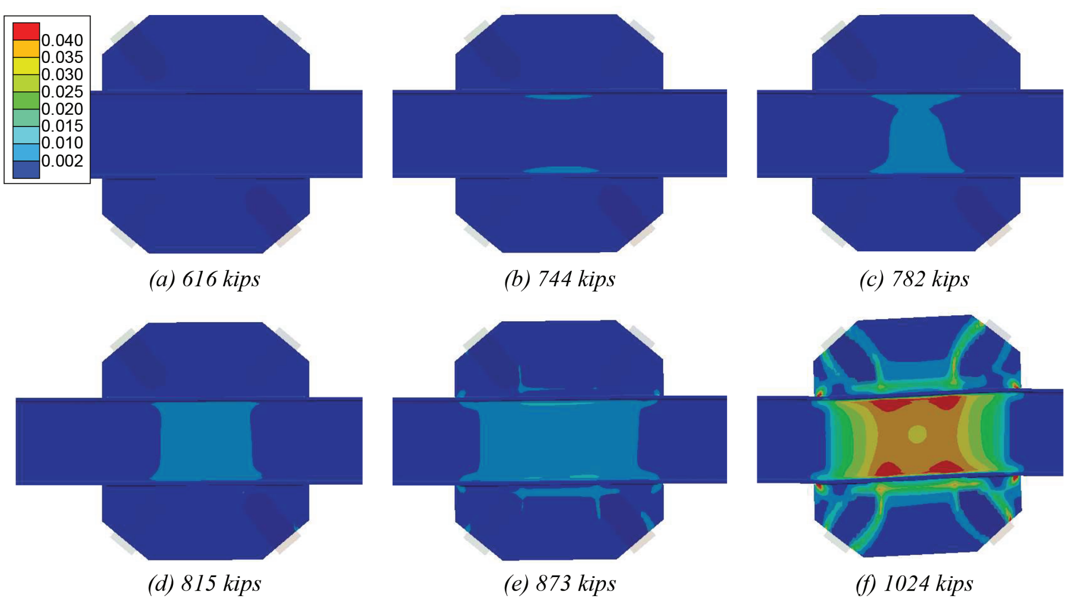


*Fig. 6. Plastic strain contours in the beam and gussets.*

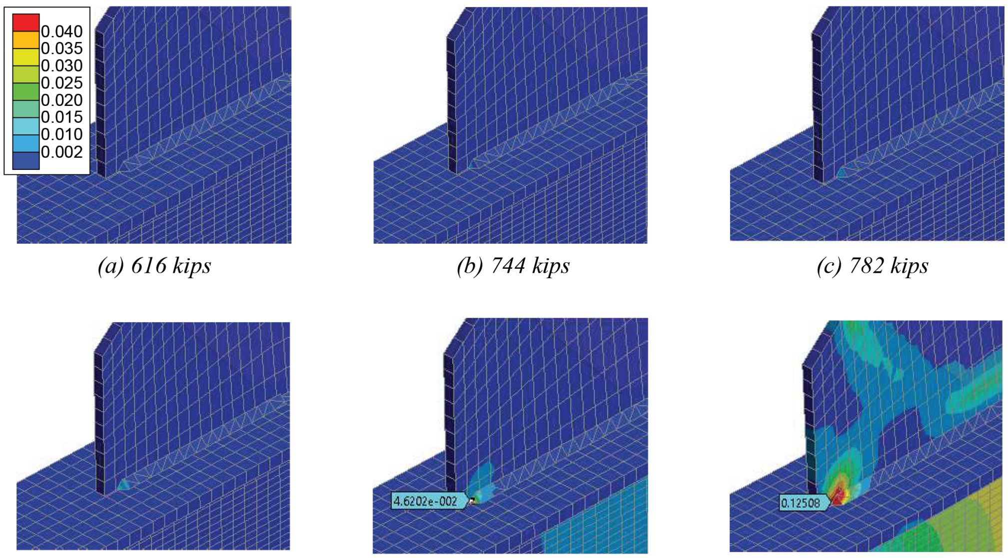


(a) 616 kips (b) 744 kips (c) 782 kips

(d) 815 kips (e) 873 kips (f) 1024 kips

*Fig. 7. Plastic strains at the gusset-to-beam welds (beam flange elements have 1 in. edge length).*

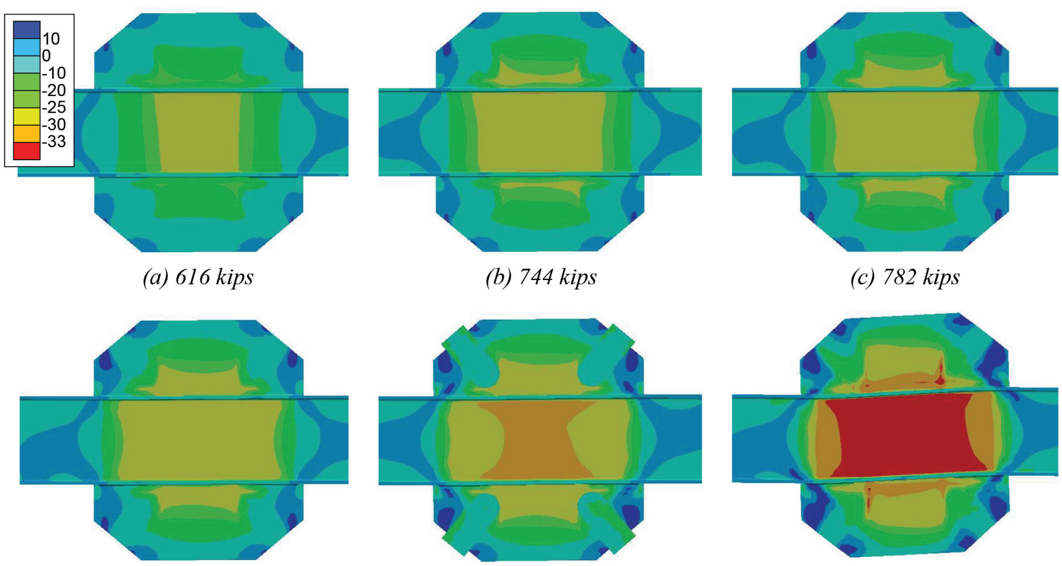


(a) 616 kips (b) 744 kips (c) 782 kips

(d) 815 kips (e) 873 kips (f) 1024 kips

*Fig. 8. Shear stresses (ksi) in the beam and gussets.*

to the stable post-yield stiffness by 873 kips. The plastic strain plot [Figure 6(c)] shows that at 782 kips, localized plastic strains above 0.002 had coalesced at the center of the beam. These strains propagated outward, with the beam web yielding being fully developed by 873 kips.

It is difficult to quantify precisely where the beam shear yielding limit state was reached, but Figure 10 offers additional insight. Figure 10 shows the tangent stiffness, $k_t$, normalized by the elastic stiffness $k_{elastic}$ for the different levels of lateral force. There appears to be an inflection point around 815 kips that suggests that the yielding is mature. As a sidenote for Figure 10, the stabilized post-yield stiffness (lateral forces greater than 900 kips) was about 10% of the elastic stiffness, even though the material hardening was only 1% of elastic because of the ratio of plastic beam rotation to story drift (to be discussed in the next section).

All these results support the conclusion that the CSM used by Sabelli and Saxey (2021) is reasonable for design.

The stress and strain contours in Figures 7 through 9 suggest some refinements for the CSM. In the CSM example,

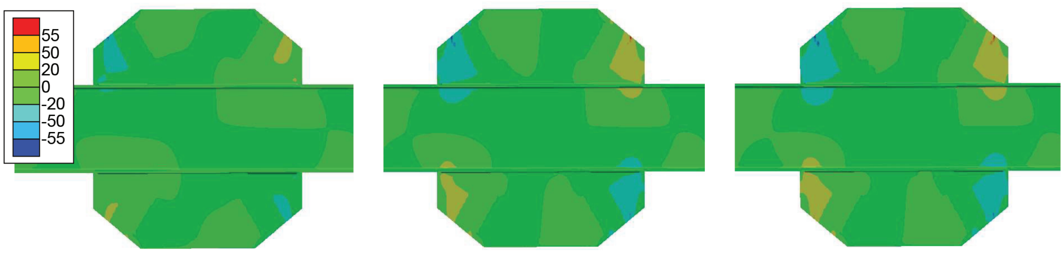

*(a) 616 kips* *(b) 744 kips* *(c) 782 kips*

*(d) 815 kips* *(e) 873 kips* *(f) 1024 kips*

*Fig. 9. Normal stresses (ksi) in the beam and gussets.*

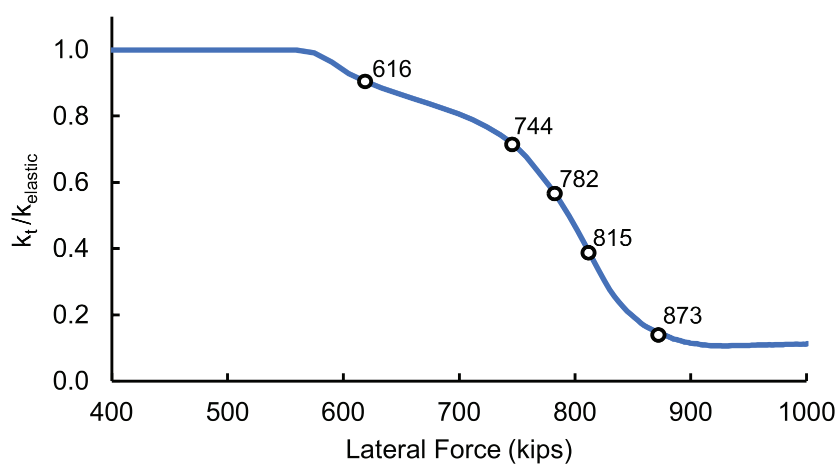


*Fig. 10. Normalized tangent stiffness corresponding to various levels of lateral force.*

a $z_1$ distance of 7.38 in. was used in design to designate the region of the gusset that is assumed to resist the moment at the connection through concentrated normal stresses. The FE model (Figures 7 and 9) indicated that the actual region of concentrated normal stress was somewhat smaller, more like 5.0 in. Another point of possible refinement is the assumption of the length that is effective for shear transfer. In the CSM example, the gusset-to-beam shear is assumed to be transferred evenly over the entire length of the gusset plate. The FE model demonstrated, as did Richards et al. (2018), that $z$ regions did not transmit much shear. A refined CSM, with smaller $z$ and shear transfer only in-between $z$ regions, may better predict the demands on the gusset-to-beam welds.

## BROADER DISCUSSION OF BEAM SHEAR YIELDING AND COMPARISON TO EBF

The CSM example frame would not be expected to experience significant beam yielding because the forces that could be delivered by the braces were lower than the forces required to reach the beam shear limit state. However, there may be other braced frames where local shear demands were not considered in the design and a beam yielding mechanism might occur. It is also possible that someone might contemplate a new seismic system that intentionally yields the beam. In those contexts, results about the extreme post-yield behavior of concentrically braced frames with beam yielding may be of interest.

The evolution of the shear stress in the beam web (Figure 8) is similar to that documented in experimental and finite element studies of shear-yielding links in eccentrically braced frames (EBF) (Hjelmstad and Popov, 1983; Richards et al., 2007). In discussing the post-yield behavior of a concentrically braced frame (CBF) with beam yielding, it is informative to compare and contrast with an EBF. An EBF FE model was developed to make comparisons with the CBF FE model as an academic exercise, see Figure 11.

The EBF model did not represent a code-compliant seismic design, just as the CBF model with a yielding beam did not represent a code-compliant seismic design. The purpose of the academic exercise was to compare and contrast beam yielding mechanisms. The EBF FE model had the same beam size (W24×94), beam length, and story heights as the CBF (Figure 5). The length of the shear link was 44 in. to match the observed intense yielding region in the CBF [Figure 5(f), red region]. The braces were modeled with elastic truss elements (infinitely strong, LINK180). As with the CBF model, the beam web and gusset plates were restrained against out-of-plane deformations, so stiffeners in the link beam or on the gussets were not necessary in the model. The nonlinear material properties for the beam were the same in the EBF model as they were in the CBF.

Figure 12 compares the inelastic pushover curves for both models. Results are shown up to an inelastic drift of 0.004. The lateral force that was required to yield the EBF was substantially lower than for the CBF with the same beam size because the eccentricity of the brace work points in the EBF was a more direct and effective way to impose shear on the beam web. Also, the CBF gussets help to carry some shear, as determined using the CSM. The lower post-yield stiffness in the EBF was a reflection of lower strains in the beam (less strain hardening).

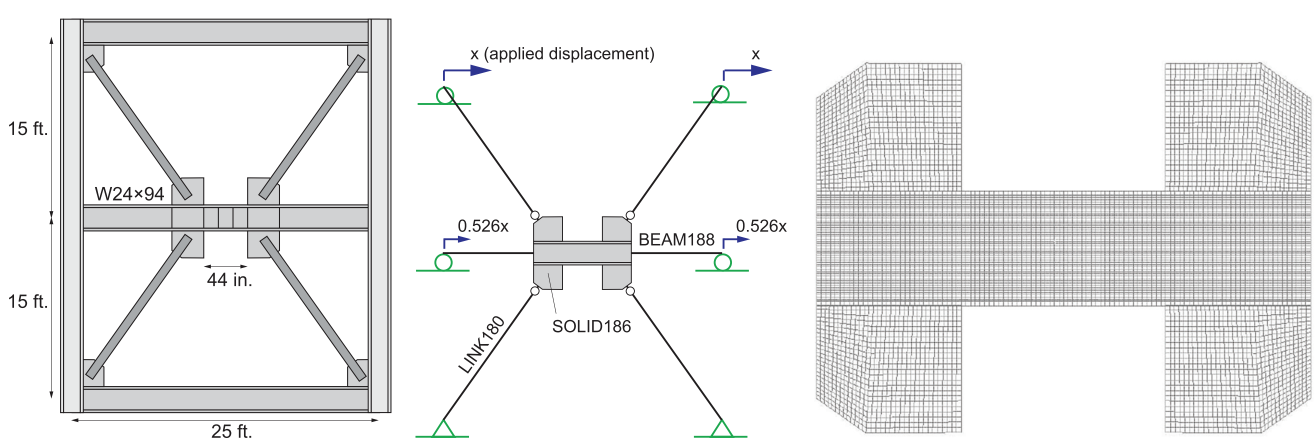

(a) Geometry (b) FE model boundary conditions (c) FE mesh

*Fig. 11. EBF frame for comparison with the CBF.*

Figure 13 compares the inelastic beam rotations versus the inelastic story drift for CBF and EBF. The EBF relationship between inelastic beam rotation and inelastic drift was within 13% of an estimate from a rigid plastic mechanism (Figure C-F3.4, AISC, 2016). The higher inelastic beam rotations for the CBF for a particular inelastic drift would make the CBF less attractive than EBF for an intentional beam yielding mechanism unless high post-yield stiffness were the primary aim.

Figure 14 compares the plastic strains and deformed geometries of both models at 0.004 rad inelastic story drift. The displacements have been scaled by a factor of 6 in both cases to illustrate the plastic mechanisms. The maximum web plastic strain in the CBF (0.035) is 75% more than the maximum plastic strain in the EBF (0.020) at the same inelastic drift. Also, the plastic strains are more uniformly distributed in the EBF.

The plastic mechanism in Figure 14 has the same form as the one postulated by Sabelli and Bolin (2022), where the plastic section of the beam is less than the full length of the gusset. The plastic strains in the gusset in Figure 14(a), including the concentrations of strain at the ends, illustrate the gusset/weld deformations required for compatibility with the yielding beam.

This academic exercise demonstrates that it is theoretically possible to design a CBF with a beam yielding mechanism, even though current seismic design provisions do not allow it. There are advantages and disadvantages of CBF

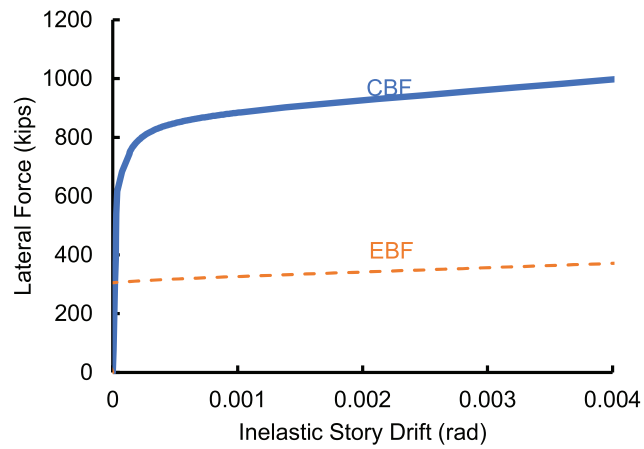


*Fig. 12. Inelastic story drift vs. lateral force for CBF and EBF.*

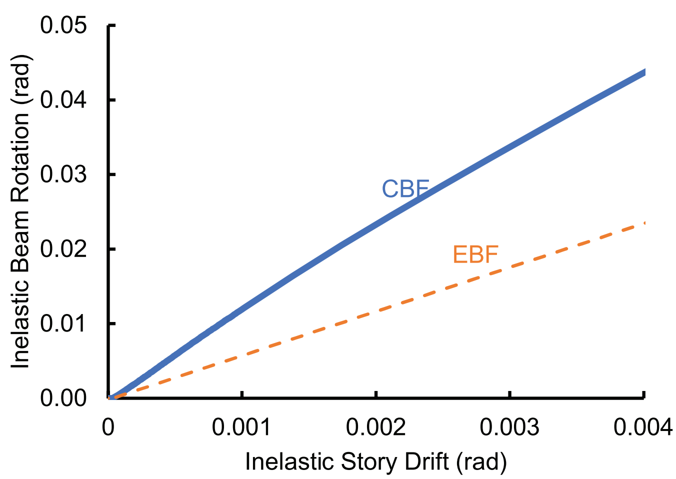


*Fig. 13. Inelastic beam rotation vs. inelastic story drift for CBF and EBF FE models.*

with beam yielding as compared to an EBF. The CBF advantages are greater elastic stiffness, strength, and post-yield stiffness. The CBF disadvantages are higher beam rotation and higher beam strains to achieve a particular inelastic drift (although less inelastic drift might be required for a CBF since the elastic stiffness is greater).

If existing chevron frames have been unintentionally designed such that yielding would occur in the beam web, these analyses demonstrate the expected plastic mechanism.

## CONCLUSIONS

A finite element (FE) model was developed to investigate the design procedure presented by Sabelli and Saxey (2021). The braces in the model had unlimited strength to force a beam-yielding mechanism to occur. A pushover analysis was performed to check if the Concentrated Stress Method (CSM) used by Sabelli and Saxey (2021) in their CSM example was accurate in predicting the beam shear yielding limit state. Here are the conclusions from the exercise:

- The CSM used by Sabelli and Saxey (2021) was reasonable for design. The FE model confirmed that the CSM example frame would not have experienced a beam yielding limit state under the design forces (maximum forces that could be delivered by the braces).
- While there was not a clear method for defining when the beam yielding limit state was reached in the FE model, an inflection point for the tangent stiffness suggested about 815 kips, which was 4% higher than the design force used in the CSM example.
- The method for estimating the $z$ regions in the CSM example might be refined. A higher value for $z$ was used in the CSM example than observed in the FE model.
- The method for assigning regions of the gusset to transmit shear in the CSM example might be refined. In the CSM example, shear was assumed to be transmitted along the entire length of the gusset, but the FE models indicate the $z$ regions are not effective for shear transfer.

An additional FE model of an EBF was used for an academic exercise, comparing the post-yield plastic mechanism of a CBF (with beam yielding) with an EBF with the same beam. This discussion was outside the scope of Sabelli and Saxey (2021) but pertinent to the broader topic of local member shear demands. Conclusions were as follows:

- The CBF FE model developed the plastic mechanism discussed by Sabelli and Bolin (2022) and confirmed their assumption that the yielding region of the beam was shorter than the total gusset length.
- The shear yielding mechanism in the CBF beam (when braces had unlimited strength), was similar to an EBF shear link; however, the lateral forces to trigger the mechanism were much higher for the CBF. At the same inelastic story drift, the inelastic beam rotation and plastic strains were higher in the CBF with beam yielding than in the EBF with the same beam size.

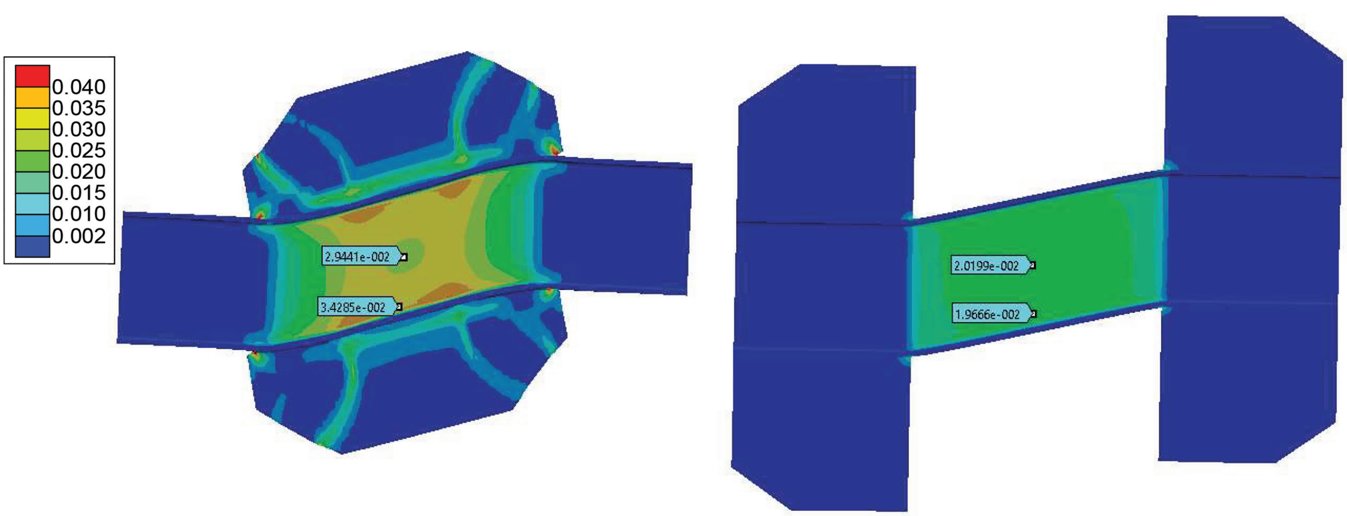


(a) Chevron (b) EBF

*Fig. 14. Plastic strains in the chevron and EBF models at 0.004 rad inelastic story drift.*

## REFERENCES


AISC (2016), *Seismic Provisions for Structural Steel Buildings*, ANSI/AISC 341-16, American Institute of Steel Construction Chicago, Ill.

ANSYS (2022), Ansys Mechanical, Release 22.1, Help System, ANSYS, Inc.

Fortney, P.J. and Thornton, W.A. (2015), "The Chevron Effect—Not an Isolated Problem," *Engineering Journal*, Vol. 52, No. 2, pp. 125–164.

Fortney, P.J. and Thornton, W.A. (2017), "The Chevron Effect and the Analysis of Chevron Beams—A Paradigm Shift," *Engineering Journal*, Vol. 54, No. 4, pp. 263–296.

Hadad, A.A. and Fortney, P.J. (2020), "Investigation on the Performance of a Mathematical Model to Analyze Concentrically Braced Frame Beams with V-Type Bracing Configurations," *Engineering Journal*, Vol. 57, No. 2, pp. 91–108.

Hadad, A.A. and Thornton, W.A. (2022), "Closure: Investigation on the Performance of a Mathematical Model to Analyze Concentrically Braced Frame Beams with V-Type Bracing Configurations," *Engineering Journal*, Vol. 59, No. 1, pp. 1–4.

Hjelmstad, K.D. and Popov, E.P. (1983), "Cyclic Behavior and Design of Link Beams," *Journal of Structural Engineering*, Vol. 109, No. 10, pp. 2,387–2,403.

Richards, P.W., Miller, B., and Linford, J. (2018), "Finite Element Evaluation of the Chevron Effect in Braced Frames," SSRP-2018/02, Brigham Young University, Provo, Utah.

Richards, P., Okazaki, T., Engelhardt, M., and Uang, C.-M. (2007), "Impact of Recent Research Findings on Eccentrically Braced Frame Design," *Engineering Journal*, Vol. 44, No. 1, pp. 41–53.

Roeder, C.W., Lehman, D.E., Tan, Q., Berman, J.W., and Sen, A.D. (2021), "Discussion: Investigation on the Performance of a Mathematical Model to Analyze Concetrically Braced Frame Beams with V-Type Bracing Configurations," *Engineering Journal*, Vol. 58, No. 1.

Sabelli, R. and Bolin, E. (2022), "The Chevron Effect: Reserve Strength of Existing Chevron Frames," *Engineering Journal*, Vol. 59, No. 3, pp. 209–224.

Sabelli, R. and Saxey, B. (2021), "Design for Local Member Shear at Brace and Diagonal-Member Connections: Full-Height and Chevron Gussets," *Engineering Journal*, Vol. 58, No. 1, pp. 45–78.

Sabelli, R., Saxey, B., Li, C.-H., and Thornton, W. A. (2021), "Design for Local Web Shear at Brace Connections: An Adaptation of the Uniform Force Method," *Engineering Journal*, Vol. 58, No. 4, pp. 223–266.